April 2018

Synthesis of Hafnium-Free Nanostructured Half-Heusler Materials for Thermoelectric Applications

Samuel V. Pedersen
Boise State University

Yanliang Zhang
University of Notre Dame

Darryl P. Butt
University of Utah

Brian J. Jaques
Boise State University

Synthesis of Hafnium-Free Nanostructured Half-Heusler Materials for Thermoelectric Applications

Abstract

Half-Heusler thermoelectric materials convert heat directly into electricity by means of the Seebeck effect. Improving the conversion efficiency and reducing fabrication costs will reduce the price per watt enabling widespread commercialization for waste heat energy harvesting and self-powered devices. In this work, a rapid low-cost synthesis route utilizing mechanical alloying via high energy planetary ball milling and spark plasma sintering was used to fabricate n-type hafnium-free single phase nano-grained TiZrNiSnSb based half-heusler monoliths with a modest figure of merit performance with significantly reduced thermal conductivity.

Synthesis of Hafnium-Free Nanostructured Half-Heusler Materials for Thermoelectric Applications

Samuel V. Pedersen[1,2], Yanliang Zhang[3], Darryl P. Butt[1,4], Brian J. Jaques[1,2]

BOISE STATE UNIVERSITY
COLLEGE OF ENGINEERING
Micron School of Materials Science and Engineering

ADVANCED MATERIALS LABORATORY
MATERIALS FOR EXTREME ENVIRONMENTS AT BOISE STATE UNIVERSITY

Introduction and Background

- Thermoelectric (TE) devices convert heat absorbed into electricity with no moving parts
- Reliable, zero-maintenance, scalable operation up to 1300K
- TE devices are needed in nuclear industry for harvesting heat to power wireless sensors
- Half-Heusler alloys are semiconductors with modest conversion efficiency
- State-of-the-Art devices use Hafnium (10X $ of Zirconium); investigated a Ti/Zr alternative

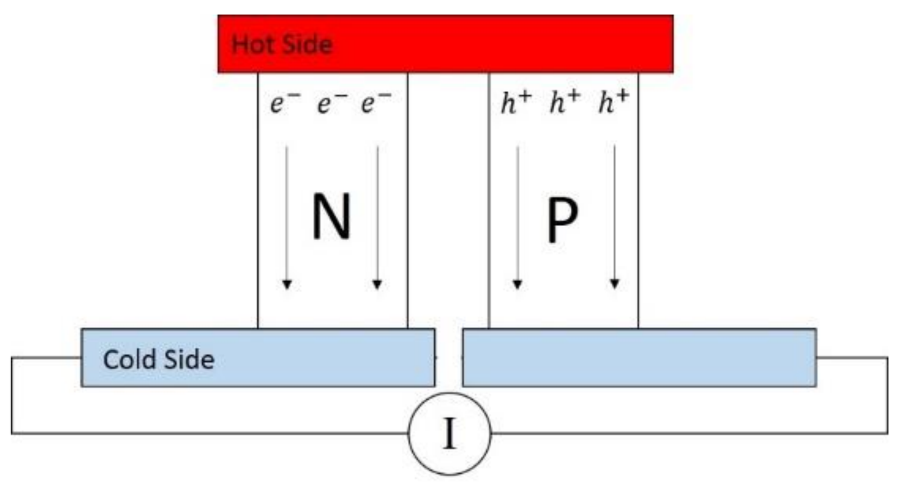

Figure 1. Thermoelectric device operating principle

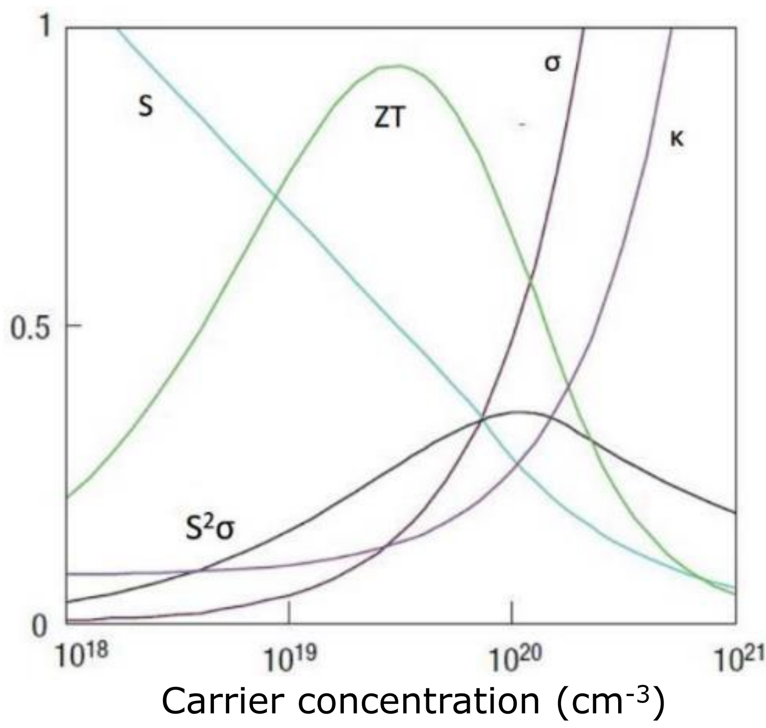

Figure 2. ZT parameter interdependency on carrier concentration[1]

The ZT is the performance figure of merit; a higher ZT indicates higher conversion efficiency

$$ZT = \frac{S^2\sigma}{K_{(e+l)}}T = \frac{S^2}{\alpha\rho_M\rho_R C_p}T$$

S: Seebeck coefficient ($^V/_K$) — σ: electrical conductivity ($^S/_m$)
k: thermal conductivity ($^W/_{mK}$) — T: absolute temperature (K)
ρ_R: electrical resistivity (Ωm) — ρ_M: mass density ($^g/_{cm^3}$)
α: thermal diffusivity (m²/s) — C_p: Specific heat capacity ($^J/_{kgK}$)

Heat capacity given by Kopp–Neumann law:

$$C_p = \sum C_i f_i$$

C_i: elemental heat capacity
f_i: mass fraction

Half-Heusler Thermoelectric Materials

Half-Heusler
- XYZ 1:1:1 stoichiometry
- 4/8 vacant 4c sites
- 18 valence electrons gives semiconductor behavior
- Ionic rock salt & covalent zinc blende bonding

Full-Heusler
- XY_2Z 1:2:1 stoichiometry
- No vacant 4c sites

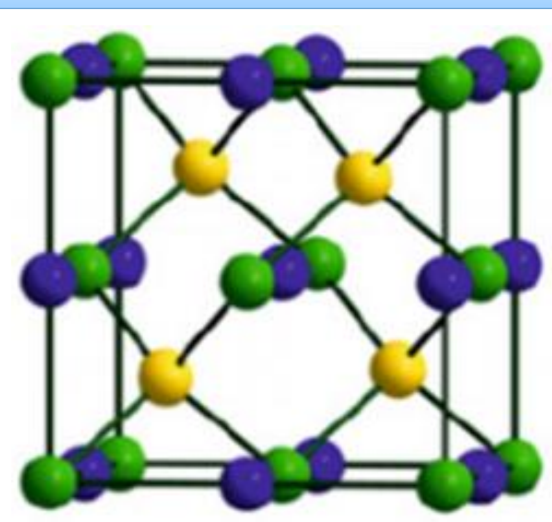

	N-type	P-type
4a	Nb/Ti/Zr/Hf	Nb/Ti
4b	Sn/Sb	Sb
4c	Ni	Fe

Figure 3: Half-heusler unit cell Space group: F4/3m, No. 216 Wycoff positions[2]: 4a (0,0,0) 4b (½ ½ ½) 4c (¼ ¼ ¼)

Advantages
- Intermediate service temperatures (700K)[2]
- Intermediate performance ZT≈1-1.5 [2]
- XYZ site compositional tailoring ↑ ZT
- High power factor (numerator of ZT)
- Abundant raw materials (except Hafnium)
- Low toxicity raw materials

Disadvantages
- High intrinsic thermal conductivity
- Brittle

Can reduce thermal conductivity by grain size reduction & mass disorder effects

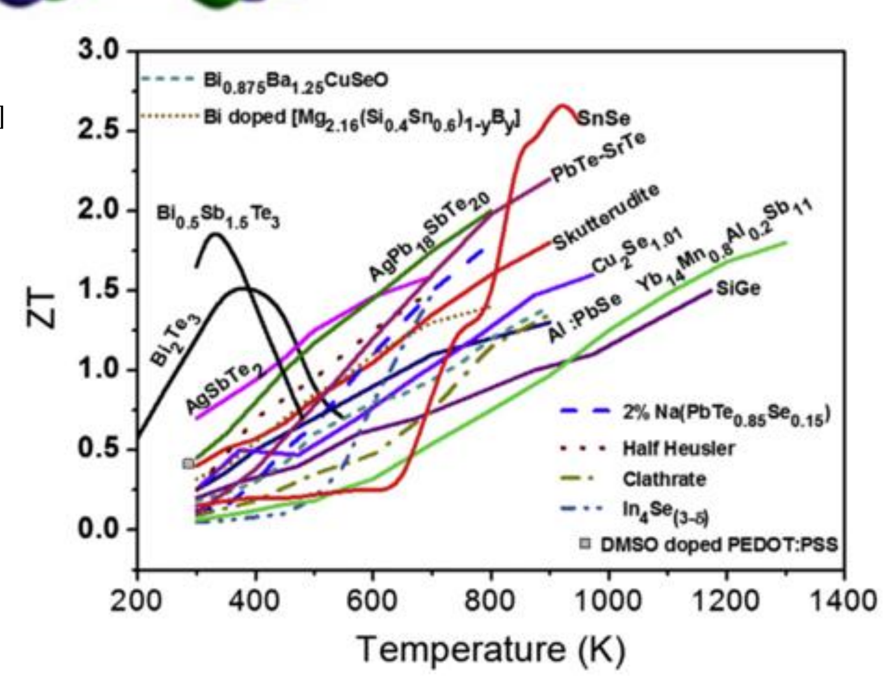

Figure 4. ZT of half-heuslers relative to other TE materials and applicable service temperatures[1]

Synthesis Route for Half-Heusler: $Ti_{0.75}Zr_{0.25}NiSn_{0.98}Sb_{0.02}$

- Mechanical alloying (MA) via ball milling uses repeated weld/fracture events to alloy powder
- Spark plasma sintering (SPS) for rapid heating under pressure to form dense nanostructured monolith

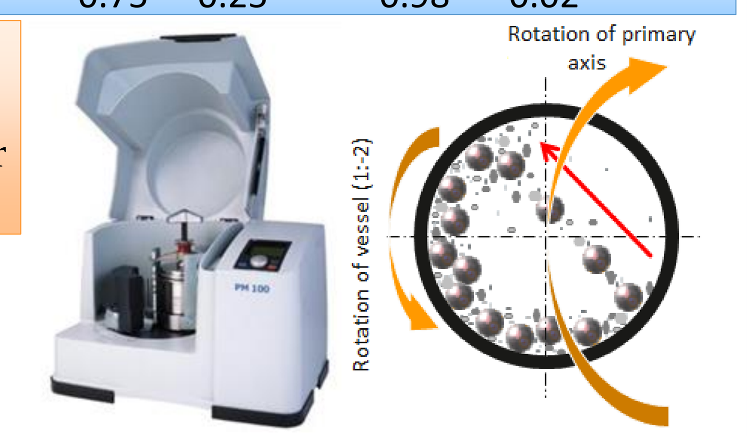

Figure 5. Planetary ball mill media cascades

High Energy Planetary Ball Milling
- Stoichiometric amounts of elemental powders
- Mill at 500 rpm for 24 hours in stainless steel 250 mL vessel filled with inert argon gas and 5 mm diameter steel media (440C) in argon
- 15:1 (media:powder) charge ratio

Spark Plasma Sintering
- Ramp 100 $^{\circ C}/_{min}$ to 800-1050 °C under 50 MPa
- Sintered under vacuum in graphite foil
- Cooled naturally to ambient temperature

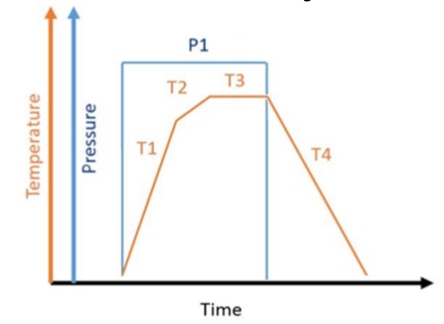

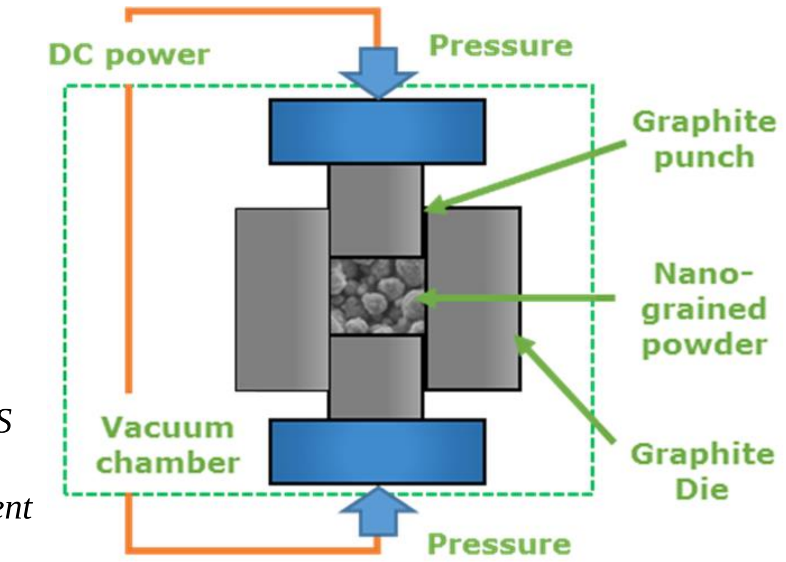

Figure 6. (left) Schematic sintering profile, (right) SPS sintering operation under vacuum and pulsed DC current

Results: Powder Characterization of $Ti_{0.75}Zr_{0.25}NiSn_{0.98}Sb_{0.02}$

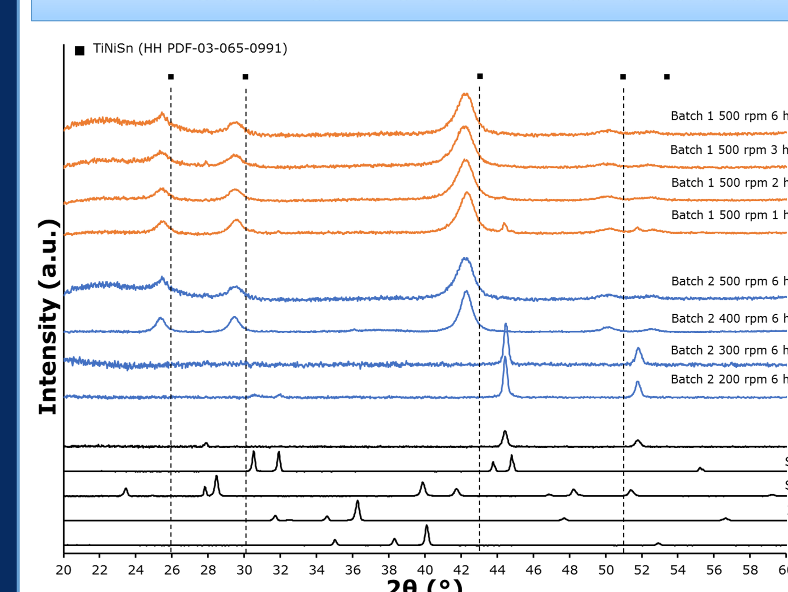

Figure 7. Powder XRD shows 400 rpm and 6 hours of milling to obtain single phase half-heusler

Powder X-ray Diffraction (XRD)
- Phases (minimum energy for HH formation)
- Peaks broaden (crystallite size decreases) with longer milling times, higher energy)
- Patterns shift due to strain, Zr substitution for Ti

Laser Scattering Particle Size Analysis (PSA)
- Suspension stability optimized with surfactants, dispersants, and ultra-sonication
- Spherical morphology distribution mean at 5 µm

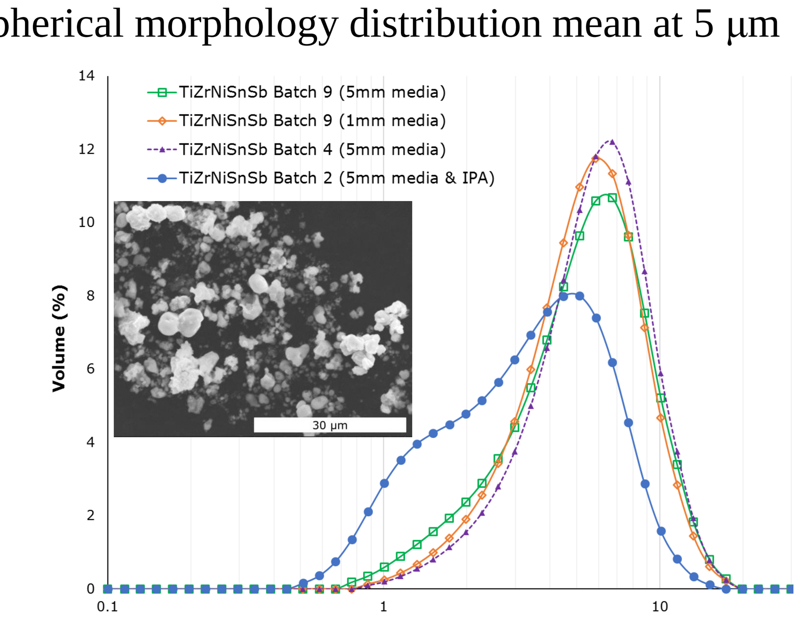

Figure 8. PSA shows changes due to wet milling; SEM shows spherical morphology

Results: Homogeneity and Composition of $Ti_{0.75}Zr_{0.25}NiSn_{0.98}Sb_{0.02}$

Energy Dispersive Spectroscopy (EDS)
- Verified HH 1:1:1 stoichiometry
- Nearly homogeneous but contains:
- Iron contamination from steel media
- Zirconium oxide inclusions
- Deleterious unreacted Ti, Ni, Sn

EDS (Atomic %)	Ti	Zr	Ni	Sn	Sb
Target	24.75	8.25	33.00	32.34	0.66
Pellet Batch 1	26	8	35	31	1
Pellet Batch 2	25	8	34	33	1

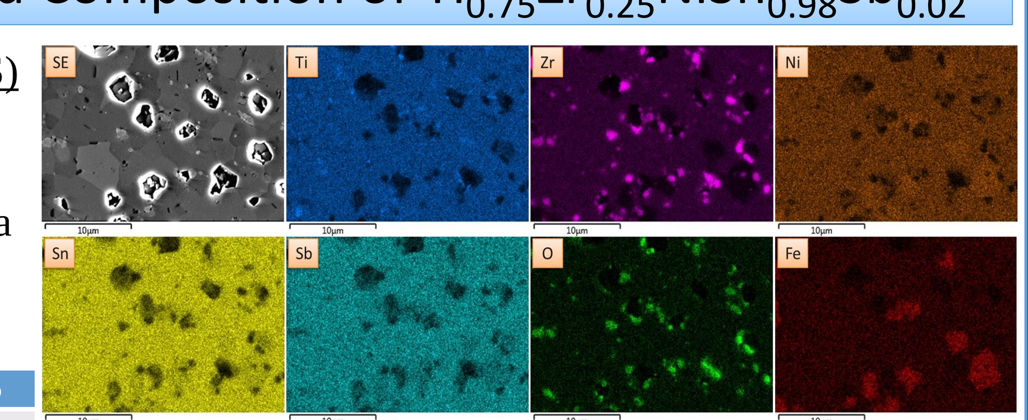

Figure 9. EDS maps on sintered pellet indicates ZrO_2 inclusions & iron contamination from milling process

Results: Grain Size and Phase of $Ti_{0.75}Zr_{0.25}NiSn_{0.98}Sb_{0.02}$

Sintered Grain Size and Thermal Treatments
- Create nanometer/micrometer grain sizes
- Treat at 1000 °C for 2 weeks for grain growth

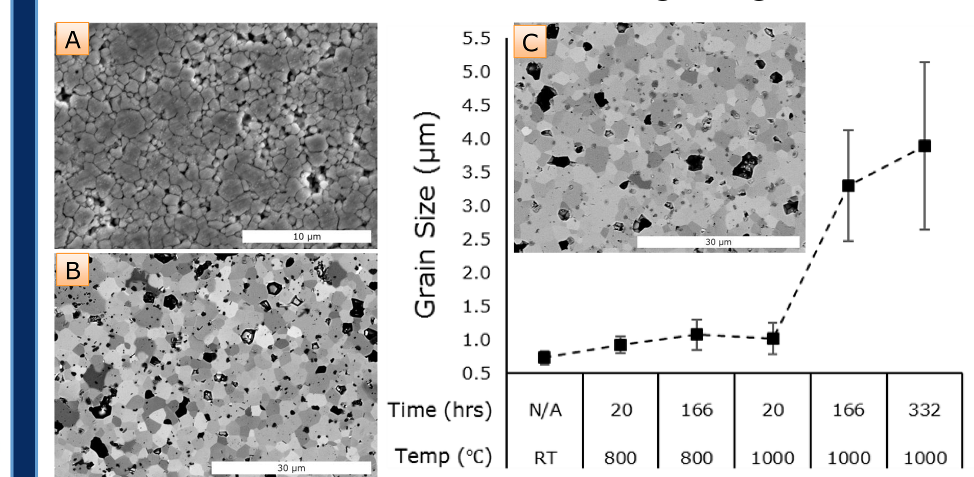

Figure 10. SEM images (A) SPS at 975 °C 10 minutes, etched (B) SPS at 1050 °C 2 minutes, unetched, (C) 975 °C sample treated 2 weeks at 1000 °C, unetched; Visible micrometer porosity ≈ 4%

Pellet XRD for Phase Identification

Figure 11. Pellet XRD of SPS at 975 °C for 10 minutes matches TiNiSn half-heusler reference, nearly single-phase purity obtained from ball milling; Impurity peaks are tin binary compounds

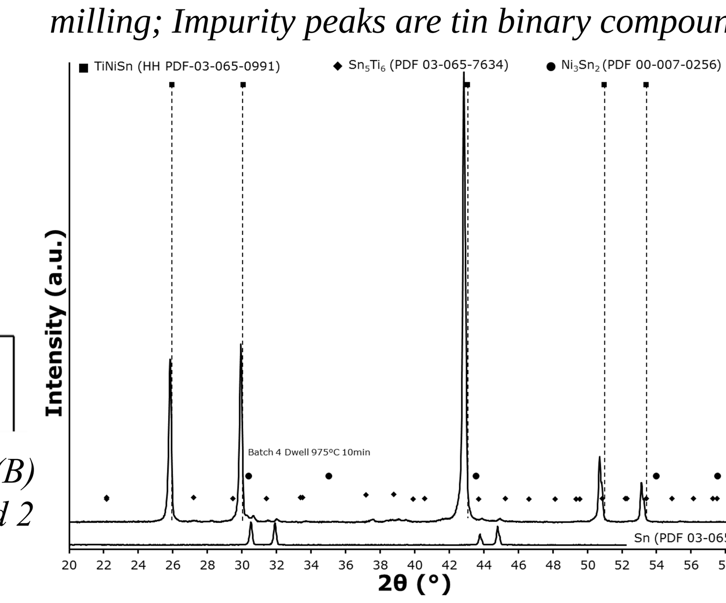

Results: Thermoelectric Performance

Comparison of Mechanical Alloy (MA) to Arc-Melt (AM) synthesis routes – MA can produce submicron grain sizes not typically seen in AM products

Figure 12. As temperature increases (A) thermal conductivity increases (B) electrical conductivity increases, (C) seebeck increases to a peak then decreases, (D) power factor increases; the reduced seebeck has a direct impact on the power factor and ZT. Reference data for the same composition synthesized using arc-melting and SPS taken from ref [3] (dotted lines with open diamonds). Lines are aids for the eye to see trends

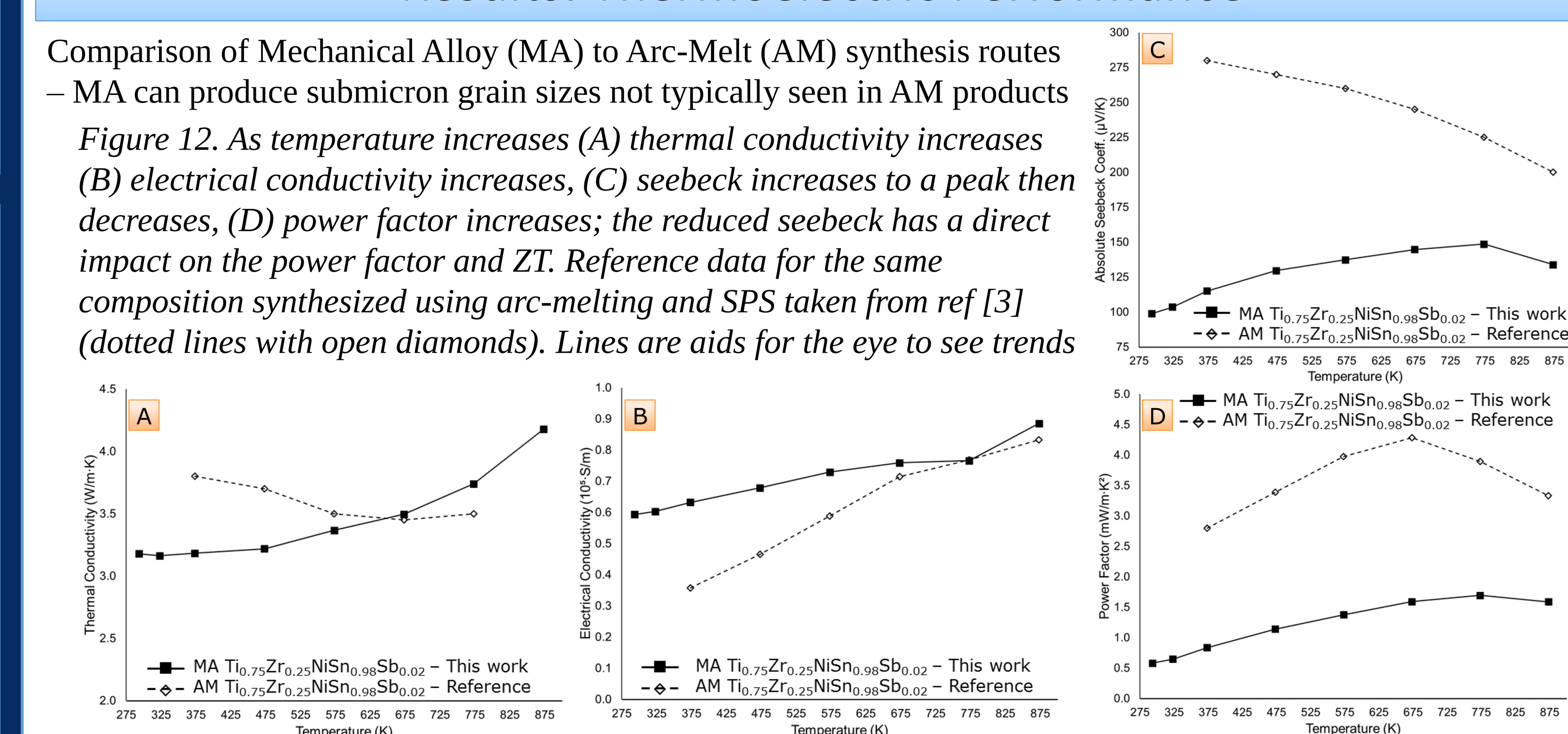

Laser Flash Analysis (LFA)
- Thermal diffusivity on 12 mm disks
- Comparable thermal conductivity

$$ZT = \frac{S^2\sigma}{K}T$$

Seebeck & Electrical Resistivity (LSR)
- Seebeck & resistivity on 12 mm disks
- Comparable electrical conductivity
- Decreased seebeck (≈60%) and power factor (≈ 60%)

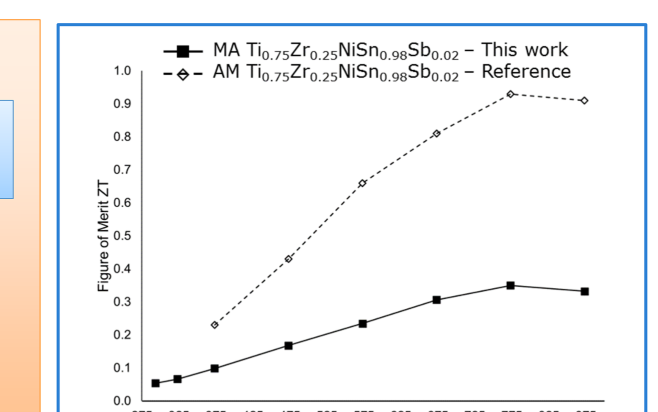

Figure 13. ZT for n-type half-heusler

Conclusion & Future Work

Figure of Merit ZT
- Peak ZT of 0.35 obtained for mechanically alloyed $Ti_{0.75}Zr_{0.25}NiSn_{0.98}Sb_{0.02}$ half-heusler
- Decreased peak ZT (~60%) for ball milled versus conventional arc-melted synthesis route
- Milling media contamination, ZrO_2 from oxygen ingress, and unreacted Ni, Ti, Sn affect carrier concentration & mobility & seebeck negatively for n-type
- Successfully alloyed Zr and Ti via ball milling; produced submicron grain size distribution

Future Work
- Milling with WC or ZrO_2 vessel/media for reduced contamination, increased milling efficiency
- Proton irradiation resistance as a function grain sizes

Contacts:
brianjaques@boisestate.edu
1. Micron School of Materials Science, Boise State University, Boise, Idaho
2. Center for Advanced Energy Studies, Idaho Falls, Idaho
3. Department of Aerospace and Mechanical Engineering, Notre Dame, Notre Dame, Indiana
4. College of Mines and Earth Sciences, University of Utah, Salt Lake City, UT

References
[1] Casper et al, Semicond. Sci. Technol. 27, 063001 (2012)
[2] Gayner et al, Prog. Mater. Sci. 83, 330–382 (2016)
[3] Gürth et al, Acta Materialia. 104, 210-222 (2016)

Acknowledgements
This work was partially funded through the United States Department of Energy, Office of Nuclear Energy, Award DENE0008255
Special Thanks To:
Bryan Forsmann, CAES; Joe Croteau, BSU

CAES Center for Advanced Energy Studies

U.S. DEPARTMENT OF ENERGY